A novel GPU-based sonar simulator for real-time applications

Abstract

Sonar simulation requires great computational effort due to the complexity of acoustic physics mainly when applied in the underwater environment. This fact turns the reproduction of sensor data into a non-trivial task. On the other hand, simulation of sonar operation data allows to evaluate algorithms and control systems without going to the real underwater environment; that reduces the costs and risks of in-field experiments. This paper proposes a novel real-time underwater imaging sonar simulator, which uses the OpenGL shading language (GLSL) chain on graphics processing unit (GPU), and is able to simulate two main types of sonar sensors: mechanical scanning imaging sonars (MSIS) and forward-looking sonars (FLS). The virtual underwater simulation was conceived based on three frameworks: (i) OpenSceneGraph (OSG) reproduces the ocean visual effects, (ii) Gazebo deals with physics effects, and (iii) the Robot Construction Kit (Rock) controls the sonar in underwater environments. The proposed sonar simulation exploits the rasterization pipeline in order to build a matrix comprised of echo intensity, distance and angular distortion, being all calculated over objects shapes in the 3D rendered scene. Sonar-intrinsic speckle noise and surface reflectance property are also considered as part of the acoustic image. Our evaluation demonstrated that the proposed method is able to operate with high frame rate, as well as realistic sonar image quality in different virtual underwater scenarios.

Key words: Simulated sensor data, sonar imaging, GPU-based processing, Robot Construction Kit (Rock), Underwater robotics.

1. Introduction

Simulation is an useful tool for designing and programming autonomous robot systems. That allows evaluating robot behavior, without dealing with physical hardware or decision-making algorithms and control systems in real-time trials, as well as costly and time-consuming field experiments.

When working with autonomous underwater vehicles (AUVs), simulation of facilities are specially relevant. AUVs usually demand expensive hardware and perform long-term data gathering operations, taking place in restrictive sites. As AUV does not need umbilical cable, and the underwater communication carries on by unreliable acoustic links, the robot should be able to make completely autonomous decisions, even with low-to-zero external assistance. While the analysis and interpretation of sensor data can be performed in a post-processing step, a real-time simulation is strongly needed for testing and evaluation of vehicle's motion responses, avoiding involved risks on real world rides.

AUVs usually act below the photic zone, with high turbidity and huge light scattering. This makes the quality of image acquisition by optical devices limited by a short range, and also artificially illuminated and clear visibility conditions. To tackle with that limitations, high-frequency sonars have been used primarily on AUVs' navigation and perception systems. Acoustic waves emitted by sonars are significantly less affected by water attenuation, aiding operation at greater ranges even as low-to-zero visibility conditions, with a fast refresh rate. Although sonar devices usually solve the main shortcomings of optical sensors, they provide noisy data of lower resolution and more difficult interpretation.

By considering sonar benefits and singularities along with the need to evaluate AUVs, recent works proposed ray tracing- and tube tracing-based techniques to simulate acoustic data with very accurate results, although having a high computational cost [1, 2, 3, 4, 5, 6, 7]. Bell [1] proposed a simulator based on optical ray tracing for underwater side-scan sonar imagery; images were generated by acoustic signals represented by rays, which are repeatedly processed, forming a 2D-array. Coiras and Groen [2] used frequency-domain signal processing to produce synthetic aperture sonar frames; in that method, the acoustic image was created by computing the Fourier transform of the acoustic pulse used to insonify the scene. For forward-looking sonar simulations, Guériot and Sintes [3] introduce a volume-based approach of energy interacting with the scene, and collected by the receiving sonar; the sound propagation is defined by series of acoustic tubes, being always orthogonal to the current sonar view, where the reverberation and objects surface irregularities are also addressed. Saç *et al.* [4] described a sonar model by computing the ray tracing in frequency domain; when a ray hits an object in 3D space, three parameters are calculated to process the acoustic data: the Euclidean distance from the sonar axis, the intensity of returned signal by Lambert Illumination model and the surface normal; the reverberation and shadow phenomena are also considered in the scene rendering. DeMarco *et al.* [5] used Gazebo and Robot Operating System (ROS) [8] integration to simulate the acoustic sound pulses by a ray tracing technique, and to produce a 3D point cloud of the coverage area; the reflected intensity has taken account of object reflectivity and the sonar image is corrupted by adding Gaussian noise, salt-and-pepper noise and median blur empirically defined. Gu *et al* [6] modeled a forward-looking device where the ultrasound beams were formed by a set of rays; the acoustic image is significantly limited by its representation us-

ing only two colors: white, when the ray strikes an object, and black for shadow areas. Kwak *et al.* [7] evolved the previous approach by adding a sound pressure attenuation to produce the gray-scale sonar frame, while the other physical characteristics related to sound transmission are disregarded.

1.1. Contributions

This paper introduces a novel imaging sonar simulator, that can overcome the main limitations of the existing approaches. As opposed to [1, 2, 3, 4, 5, 6, 7], where the proposed models simulate a specific sonar type, our model is able to reproduce two kind of sonar devices: mechanical scanning imaging sonar (MSIS) and forward-looking sonar (FLS). Also, the underwater scene is processed during the pipeline rendering on graphics processing unit (GPU), accelerating the simulation process, guaranteeing real-time simulation, in contrast to the methods found in [1, 2, 4, 5]. The intensity measured back from the insonified objects depends on the accumulated energy based on surface normal directions, producing more realistic simulated scenes, instead of statically defined by the user, as in [5], or in a binary representation as found in [6, 7]. The speckle noise is modeled as a non-uniform Gaussian distribution and applied to the final sonar image, performing a more realistic sensing, differently to [3, 4, 6, 7].

The main goal here is to build quality and low time-consuming acoustic frames, according to underwater sonar image formation and operation modes (see Section 2). The shader matrix with depth and normal buffers, and angular distortion values are extracted from underwater scene during the rasterization pipeline, and subsequently fused to generate the simulated sonar data, as described in Section 3. Qualitative and time evaluation results for two different sonar devices are presented in Section 4, and allow for the use of the proposed simulator in real-time applications.

2. Imaging Sonar operation

Sonars are echo-ranging devices that use acoustic energy to locate and survey objects in a desired area. The sonar transducer emits pulses of sound waves (or ping) until they hit with any object or be completely absorbed. When the acoustic signal collides with a surface, part of this energy is reflected, while other is refracted. The sonar data is built by plotting the echo measured back versus time of acoustic signal. The transducer reading in a given direction forms a *beam*. A single beam transmitted from a sonar is illustrated in Fig. 1. The horizontal and vertical beamwidths are represented by the azimuth ψ and elevation θ angles, respectively, where each sampling along the beam is named as *bin*. The sonar coverage area is defined by R_{min} and R_{max}. Since the speed of sound underwater is known, or can be measured, the time delay between the emitted pulses and their echoes reveal how far the objects are (distance r), as well as how fast they are moving. The backscattered acoustic power in each bin determines the intensity value.

With different azimuth directions, the array of transducer readings forms the final sonar image. Since all incoming signals converge to the same point, the reflected echoes could have been originated anywhere along the corresponding elevation arc at a fixed range, as depicted in Fig. 1. In the acoustic representation, the 3D information is lost in the projection into a 2D image.

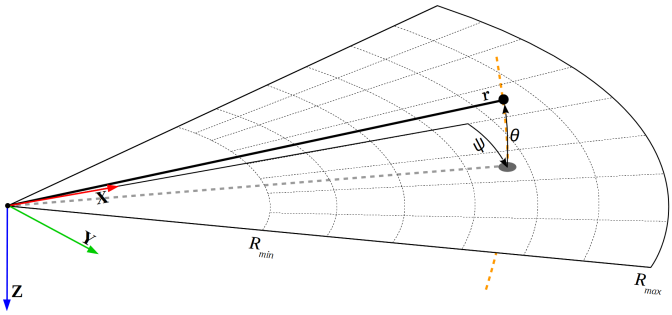

Figure 1: Imaging sonar geometry. By the projection process, all 3D points belonging to the same elevation arc (represented as dashed orange line) will be represented to the same image point in the 2D plane. In this way, range r and azimuth angle ψ are measured, and elevation angle θ is lost. The sonar coverage area is defined by R_{min} and R_{max}.

2.1. Sonar characteristics

Although sonar devices overcome the main limitations of optical sensors, they present more difficult data interpretation due to:

(a) **Shadowing**: This effect is caused by objects blocking the sound waves transmission and causing regions behind them, without acoustic feedback. These regions are defined by a black spot in the image occluding part of the scene;

(b) **Non-uniform resolution**: The amount of pixels used to represent an intensity record in the cartesian coordinate system grows as its range increases. This fact causes image distortions and object flatness;

(c) **Changes in viewpoint**: Imaging the same scene from different viewpoints can cause occlusions, shadows movements and significant alterations of observable objects [9]. For instance, when an outstanding object is insonified, its shadow is shorter, as the sonar becomes closer;

(d) **Low signal-to-noise ratio (SNR)**: The sonar suffers from low SNR mainly due the very-long-range scanning, and the presence of speckle noise introduced caused by acoustic wave interferences [10];

(e) **Reverberation**: This phenomenon is caused when multiple acoustic waves returning from the same object are detected over the same ping, producing duplicated objects.

2.2. Types of underwater sonar devices

The most common types of underwater acoustic sonars are MSIS and FLS. In the former, the sonar image is built for each pulse, with one beam per reading (see Fig. 2(a)); these sonar images are usually shown on a display pulse by pulse, and the head position reader is rotated according to motor step angle. After a full 360° sector reading (or the desired sector defined by left and right limit angles), the accumulated sonar data is

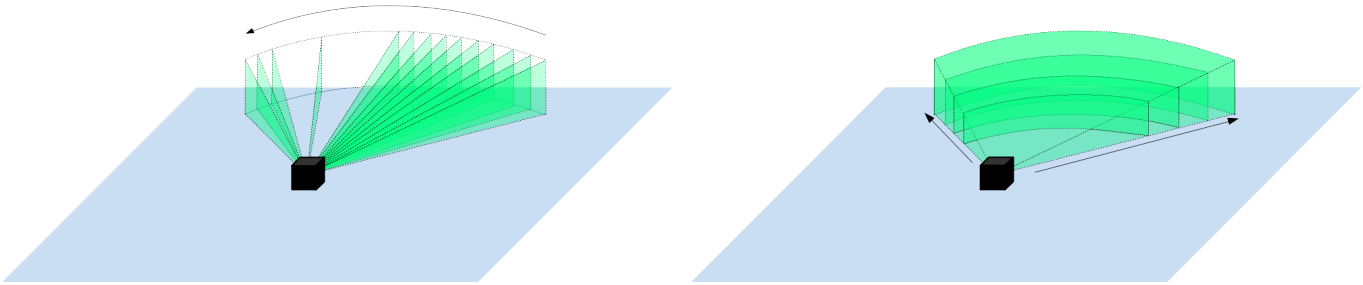

(a) (b)

Figure 2: Different underwater sonar readings: (a) From a mechanical scanning imaging sonar and (b) from a forward-looking sonar.

overwritten. The acquisition of a scanning image involves a relatively long time, introducing distortions caused by the vehicle movements. This sonar device is generally applied in obstacle avoidance [11] and navigation [12] applications.

As illustrated in Fig. 2(b), the whole forward view of a FLS is scanned and the current data is overwritten by the next one in a high frame rate, with n beams being read simultaneously. This is similar to a streaming video imagery for real-time applications. This imaging sonar is commonly used for navigation [13], mosaicing [9], target tracking [14] and 3D reconstruction [15].

3. GPU-based sonar simulation

The goal of this work is to simulate two types of underwater sonar by vertex and fragment processing, with a low computational cost. The complete pipeline of the proposed simulator, from the virtual scene to the simulated acoustic data, is seen in Fig. 3 and is detailed in the following subsections. The sonar simulation is written in C++ with OpenCV [16] support as Rock packages.

3.1. Rendering underwater scene

The Rock-Gazebo integration [17] provides the underwater scenario, and allows real-time hardware-in-the-loop simulations. In this framework, Gazebo handles the physical engines, and the Rock's visualization tools are responsible by the scene rendering. The graphical data in Rock are based on OpenSceneGraph framework, an open source C/C++ 3D graphics toolkit built on OpenGL. The osgOcean framework is used to simulate the ocean visual effects, and the ocean buoyancy is defined by the Gazebo, as described in [17].

All scene aspects, such as world model, robot parts (including sensors and joints) and other objects presented in the environment are defined by simulation description files (SDF), which use the SDFormat [18], a XML format used to describe simulated models and environments for Gazebo. Visual and collision geometries of vehicle and sensor robot are also described in specific file formats. Each component described in the SDF file becomes a Rock component, which is based on the Orocos real-time toolkit (RTT) [19], providing I/O ports, properties and operations as communication layers. When the models are loaded, Rock-Gazebo creates I/O ports to allow real-world or simulated system components interacting with the simulated models. A resulting scene sample of this integration is seen in Fig. 4.

3.2. Shader rendering

GPUs are parallel numeric computing chips specialized to speed up 2D and 3D graphics processing, reducing the computational effort of the central processing unit (CPU). The rendering pipeline can be customized by defining programs on GPU called shaders. A shader is written in OpenGL Shading Language (GLSL) [20], a high-level language with a C-based syntax which enables more direct control of graphics pipeline, which avoids the use of low-level or hardware-specific languages. Shaders can describe the characteristics of either a vertex or a fragment (a single pixel). Vertex shaders are responsible by transforming the vertex position into a screen position by the rasterizer, generating texture coordinates for texturing, and lighting the vertex to determine each color. The rasterization results in a set of pixels to be processed by fragment shaders, which manipulate their locations, depth and alpha values, and interpolated parameters from the previous stages, such as colors and textures.

In our work, the underwater scene is sampled by a virtual camera, whose optical axis is aligned with the intended viewing direction of the imaging sonar device, as well as the covered range and opening angle. By programming the fragment and vertex shaders, the sonar data is computed as:

(a) **Depth** is the camera focal length, calculated by the Euclidean distance to the object surface point;

(a) **Intensity** presents the echo reflection energy based on object surface normal angle up to the camera;

(a) **Angular distortion** is the angle formed from the camera center column up to the camera boundary column, for both directions.

All those three informations are normalized into the interval [0,1], where zero means no energy and one means maximum echo energy for intensity data, respectively. For depth data, the minimum value portrays a close object while the maximum value represents a far one, limited by the sonar maximum range.

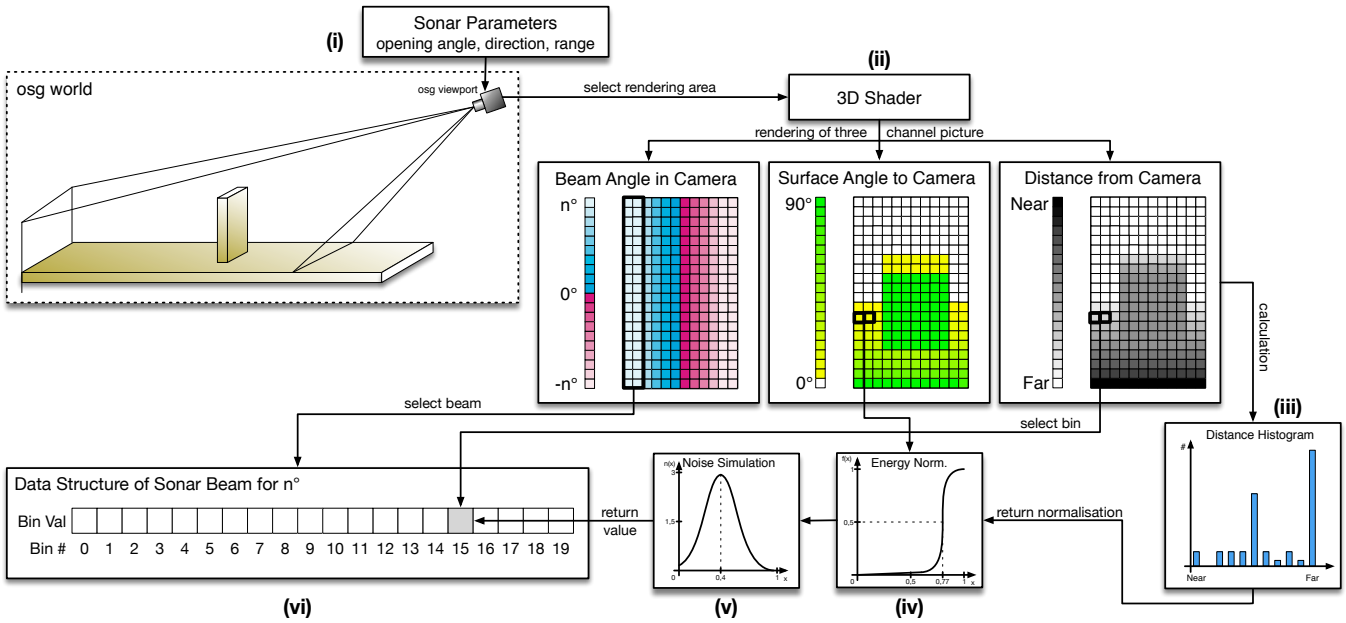

Figure 3: A graphical overview of the imaging sonar simulation process: (i) a virtual camera, specialized as the sonar device, samples the underwater scene; (ii) three components are calculated by shader rendering on GPU: the Euclidean distance from camera center, the surface normal angles, and the angular distortion; the shader information is splitted in beam parts, according the angular distortion values, and bin depth and intensity are defined by distance histogram (iii) and energy normalization (iv); (v) the speckle noise is applied to the final sonar data; (vi) and the simulated acoustic data is presented as Rock's data type.

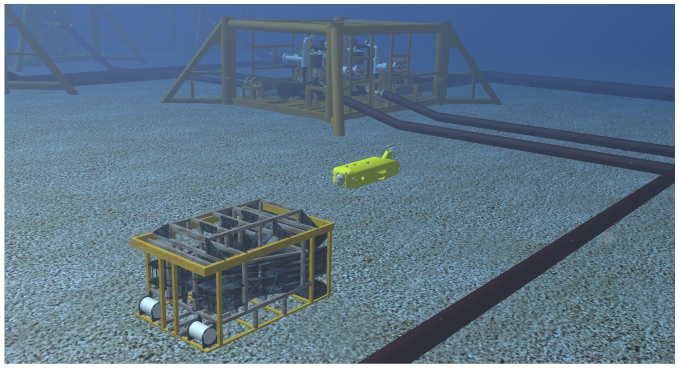

Figure 4: The AUV in Rock-Gazebo underwater scene.

Angle distortion value is zero in image center column which increases for both borders to present the half value of horizontal field of view.

In realistic sensing, real-world surfaces usually present irregularities and different reflectance values. To render that in a virtual scene, the intensity values can also be defined by a normal maps and material property information. Normal mapping is a perturbation rendering technique to simulate wrinkles and dents on the object surface by passing RGB textures and modifying the normal directions on shaders. This approach consumes less computational resources for the same level of detail, compared to the displacement mapping technique, because the geometry remains unchanged. Since normal maps are built in tangent space, interpolating the normal vertex and the texture, a tangent, bitangent and normal (TBN) matrices are computed to convert the normal values into the world space. Representation of normal mapping process in our approach is seen in Fig. 5.

The reflectance allows to properly describe the intensity received back from observable objects in shader processing, according their material properties. For instance, aluminum has more reflectance than wood and plastic. When an object has its reflectivity defined, the reflectance value ρ is passed to fragment shader and must be positive. As seen in Fig. 6, normal values are directly proportional to the reflectance value ρ. At the end, the shader process provides a matrix with three main data: Intensity, depth and angular distortion.

3.3. Simulating sonar device

The 3D shader matrix is processed in order to build the corresponding acoustic representation. Since the angular distortion is radially spaced over the horizontal field-of-view, where all pixels in the same column have the same angle value, the first step is to split the image in a number of beam parts. Each column is correlated with its respective beam, according to sonar bearings, as seen in Fig. 3. In this case, one beam represents one or more columns. Each beamed sub-image is converted into bin intensities using the depth and intensity data. In a real imaging sonar, the echo measured back is sampled over time and the bin number is proportional to the sensor range. In other words, the initial bins represent the closest distances, while the latest bins are the farthest ones. Therefore a distance histogram is evaluated to group the sub-image pixels with their respective bins, according to the depth value. This information is used to calculate the accumulated intensity of each bin.

Due to the acoustic beam spreading and absorption in the water, the final bins have less echo strength than the first ones, because the energy is lost twice, in the environment. To tackle with that issue, the sonar devices use an energy normalization

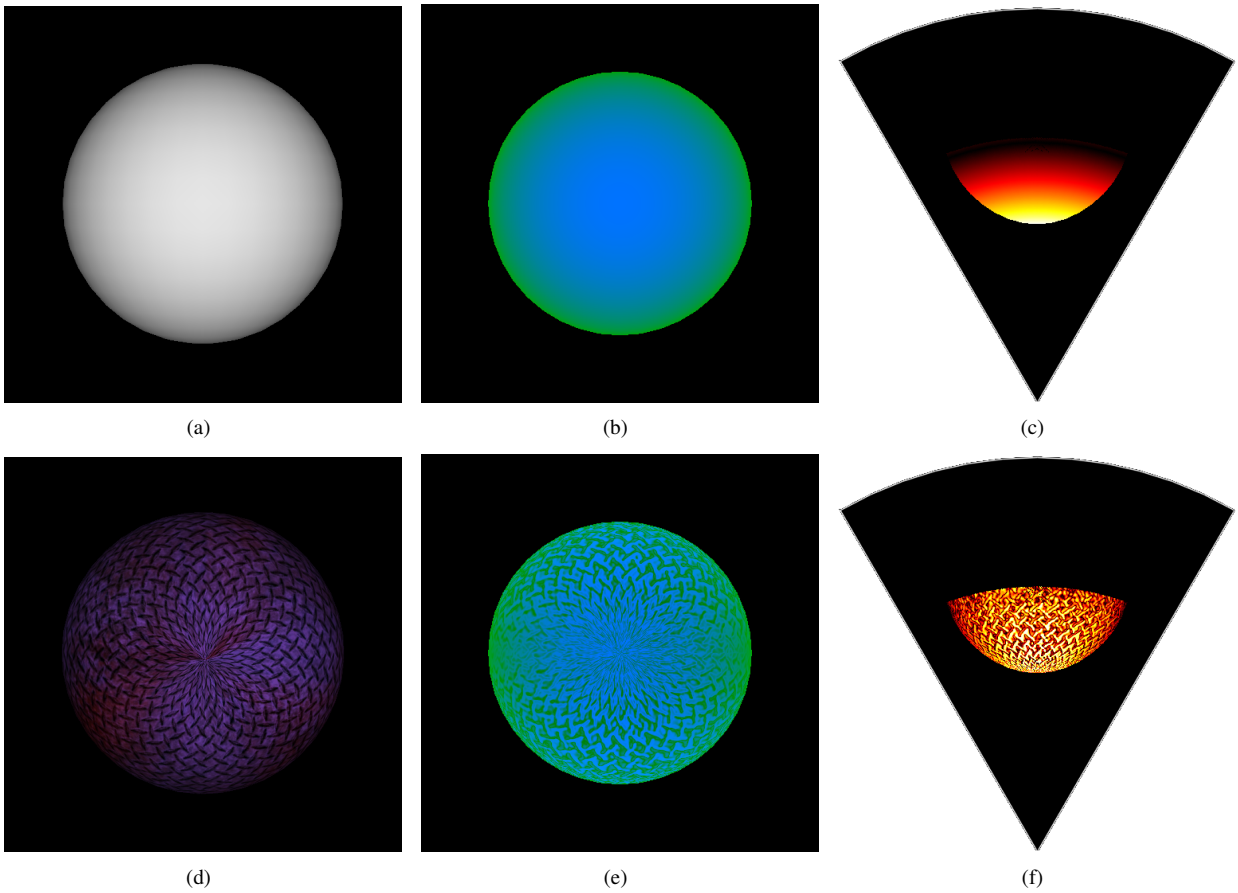

Figure 5: Example of shader rendering with normal mapping processing: A sphere without texture (a) and with texture (d); their respective shader image representation in (b) and (e), where blue is the normal channel and green is the depth one; and the final acoustic image in (c) and (f). By using normal mapping technique, the textures changes the normal directions, and the sonar image details the appearance of object surface, like in real-world sensing.

based on time-varying gain for range dependence compensation, which spreads losses in the bins. In our simulation approach, the accumulated intensity in each bin is normalized as

$$I_{bin} = \sum_{x=1}^{N} \frac{1}{N} \times S(i_x), \quad (1)$$

where I_{bin} is the intensity in the bin after energy normalization, x is the pixel location in the shader matrix, N is the distance histogram value (number of pixels) of that bin, $S(i_x)$ is a sigmoid function, and i_x is the intensity value of the pixel x.

Finally, the sonar image resolution needs to be big enough to fill all informations of the bins. For that, the number of bins involved is in direct proportion to the sonar image resolution.

3.4. Noise model

Imaging sonar systems are disturbed by a multiplicative noise known as speckle, and caused by coherent processing of backscattered signals from multiple distributed targets. These latter ones degrade image quality and the visual evaluation. Speckle noise results in constructive and destructive interferences which are shown as bright and dark dots in the image. The noisy image has been expressed as [21]:

$$y(t) = x(t) \times n(t), \quad (2)$$

where t is the time instant, $y(t)$ is the noised image, $x(t)$ is the free-noise image, $n(t)$ is the speckle noise matrix, and $\times$ symbol defines an element-wise multiplication.

This type of noise is well-modeled as a Gaussian distribution. The physical explanation is provided by the central limit theorem, which states that the sum of many independent and identically distributed random variables tends to behave a Gaussian random variable. A Gaussian distribution is defined by following a non-uniform distribution, skewed towards low values, as seen in Fig. 3, and applied as speckle noise in the simulated sonar image. After that, the simulation sonar data process is performed in each frame.

3.5. Integrating sonar device with Rock

To export and display the sonar image, the simulated data is encapsulated as Rock's sonar data type, and provided as an output I/O port of a Rock's component.

4. Simulation results and experimental analysis

To evaluate our simulator, experiments were conducted by using a 3D model of an AUV equipped with one MSIS and one FLS, studied in different scenarios. The following devices

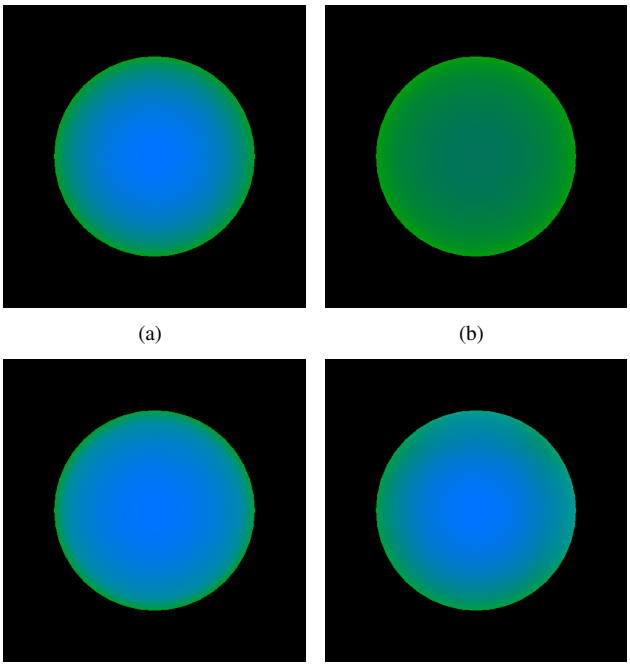

(a) (b) (c) (d)

Figure 6: Examples of different reflectance values, ρ, applied in shader image representation, where blue is the normal channel and green is the depth channel: (a) raw image; (b) $\rho = 0.35$; (c) $\rho = 1.40$; and (d) $\rho = 2.12$.

configuration are summarized in Table 1. As the scene frames are being captured by the sonars, resulting simulated acoustic images are sequentially presented, on-the-fly.

4.1. Experimental evaluation

The virtual FLS from AUV was used to insonify the scenes from three distinct scenarios. A docking station, in parallel with a pipeline on the seabed, composes **the first scenario** (see Fig. 7(a)). The target surface is well-defined in the simulated acoustic frame (see Fig. 7(b)), even as the shadows and speckle noise. Given the docking station is metal-made, the texture and reflectivity were set, such as a higher intensity shape was resulted in comparison with the other targets. **The second scenario** presents the vehicle in front of a manifold model in a non-uniform seabed (see Fig. 7(c)). The target model was insonified to generate the sonar frame from the underwater scene. The frontal face of the target, as well the portion of the seabed and the degraded data by noise, are clearly visible in the FLS image. Also, a long acoustic shadow is formed behind the manifold, occluding part of the scene. **The third scenario** contains a sub-sea isolation valve (SSIV) structure, connected to a pipeline in the bottom (see Fig. 7(e)).

Due to sensor configuration and robot position, the initial bins usually present a blind region in the three simulated scenes, caused by absence of objects at lower ranges, similar to real images. Also, the brightness of sea-floor decreases, when farthest from sonar, because of the normal orientation of the surface.

The MSIS was also simulated in three different experiments. The robot in a big textured tank composes **the first scene** (see Fig. 8(a)). Similar to the first scenario of FLS experiment,

Table 1: Sonar devices configurations used on experimental evaluation.

Device	# of beams	# of bins	Field of view	Down tilt	Motor Step
FLS	256	1000	120° x 20°	20°	-
MSIS	1	500	3° x 35°	0°	1.8°

the reflectivity and texture were set to the target. The rotation of the sonar head position, by a complete 360° scanning, produced the acoustic frame of tank walls (see Fig. 8(b)). **The second scene** involves the vehicle's movement during the data acquisition process. The scene contains a grid around the AUV (see Fig. 8(c)), a MSIS in the front of the AUV is used. This trial induces a distortion in the final acoustic frame, because the relative sensor position with respect to the surrounding object changes while the sonar image is being built (see Fig. 8(d)). In this case, the robot rotates 20° left during the scanning. **The last scene** presents the AUV over oil and gas structures on the sea bottom (see Fig. 8(e)). Using a MSIS located in the back of the AUV, with a vertical orientation, the scene was scanned to produce the acoustic visualization. As illustrated in Fig. 8(f), object surfaces present clear definition in the slice scanning of the sea-floor.

The experimental scenarios provided enough variability of specific phenomena usually found in real sonar images, such as acoustic shadows, noise interference, surface irregularities and properties, distortion during the acquisition process and gradient of acoustic intensities. However, our sonar model also presented some limitations. For instance, the speckle noise application is restricted to regions with acoustic intensity, as shown in Figs. 7(f) and 8(b). This fact is due to our sonar model, defined in Eq. 2, be multiplicative. In real sonar images, the noise also granulates the shadows and blind regions. The sonar simulator can be improved by inserting an additive noise to our model. A second feature missing in simulated acoustic images are the ghost effects caused by reverberation. This lacking part can be addressed by implementation of a multi-path propagation model.

4.2. Computational time

Performance evaluation of the simulator was determined by considering the suitability to run real-time applications. The experiments were performed on a laptop with Ubuntu 16.04 64 bits, Intel Core i7 3540M processor running at 3 GHz with 16GB DDR3 RAM memory and NVIDIA NVS 5200M video card.

The elapsed time of each sonar data is stored to compute the average time, standard deviation and frame rate metrics, after 500 iterations, as summarized in Tables 2 and 3. After changing the device parameters, such as number of bins, number of beams and field of view, the proposed approach generated the sonar frames with a high frame rate, for both sonar types. Given the Tritech Gemini 720i, a real forward-looking sonar sensor, with a field of view of 120° by 20° and 256 beams, presents a maximum update rate of 15 frames per second, the results allow

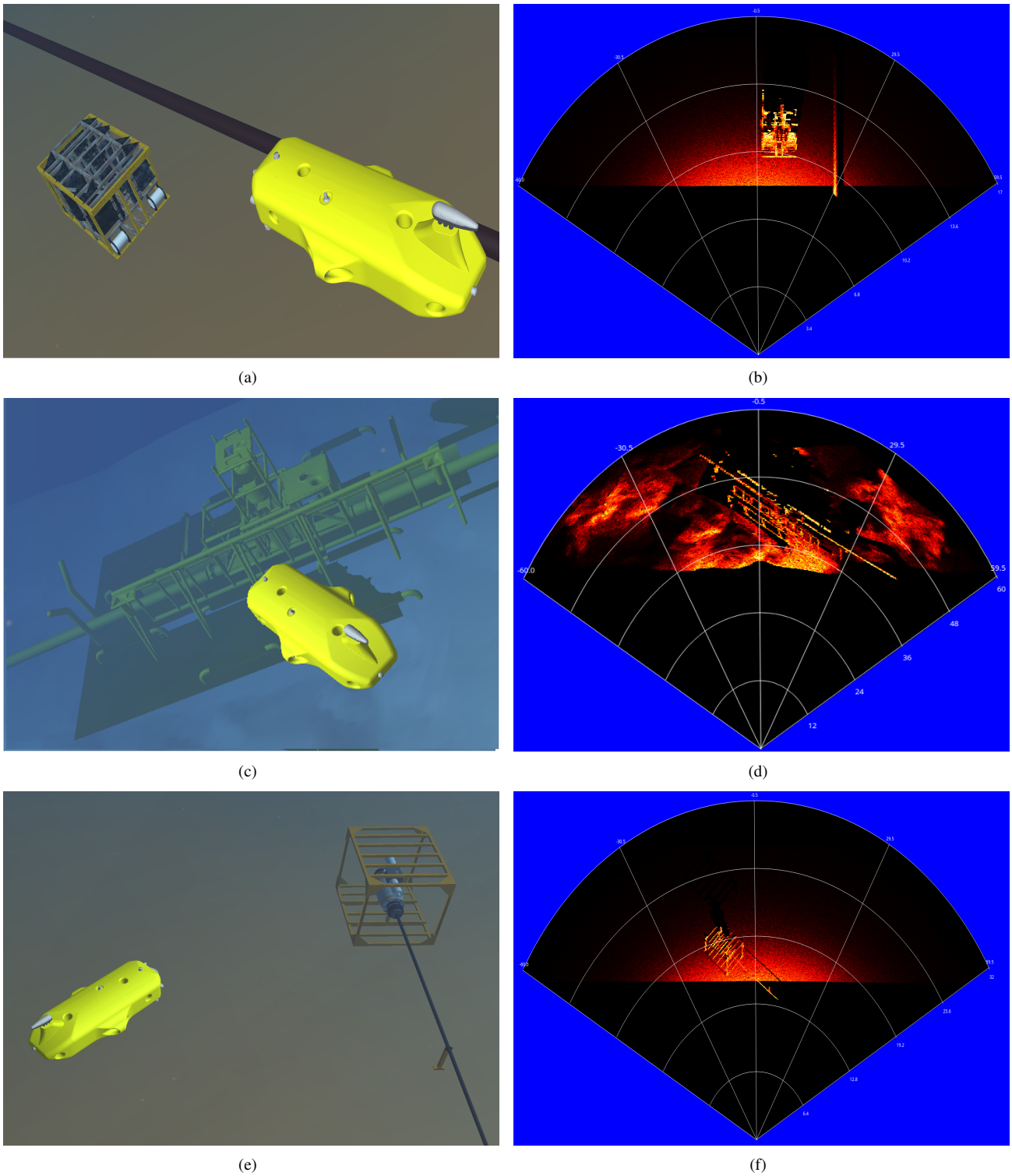

(a) (b) (c) (d) (e) (f)

Figure 7: Forward-looking sonar simulation experiments: (a), (c) and (e) present the virtual underwater trials, while (b), (d) and (f) are the following acoustic representations of each scenario, respectively.

the use of the sonar simulator for real-time applications. Also, the MSIS data built by the simulator is able to complete a 360° scan sufficiently fast in comparison with a real sonar as Tritech Micron DST. Moreover, for the FLS device, these rates are superior to the rates lists by DeMarco *et al* [5] (330*ms*) and Saç *et al* [4] (2.5*min*). For MSIS type, to the best of our knowledge, there is no previous work done for comparison.

According to previous results, since the number of bins is directly proportional to sonar image resolution, as explained in Section 3.3, this is also correlated with the computational time.

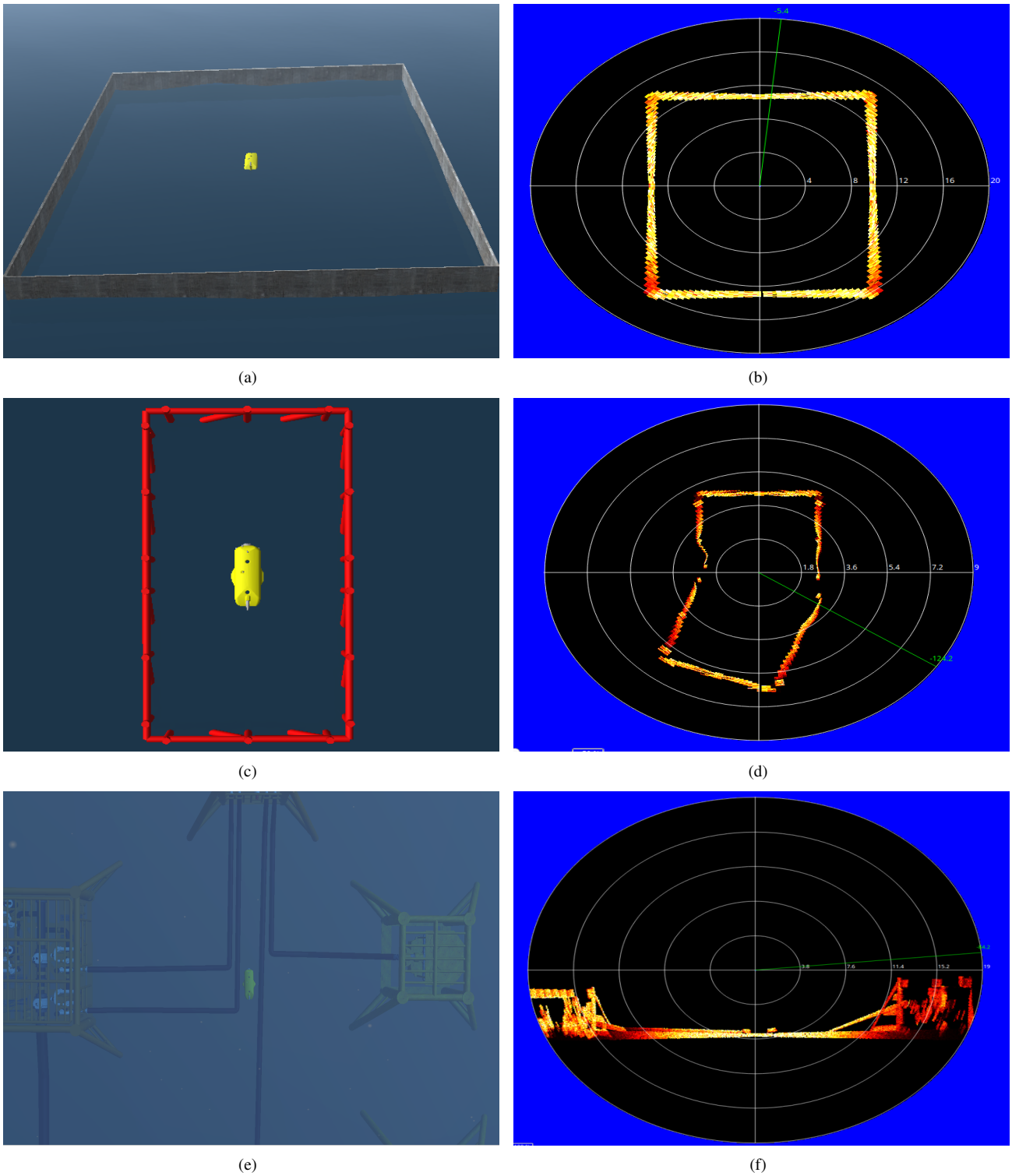

Figure 8: Experiments using mechanical scanning imaging sonar in three different scenarios (a), (c) and (e), and the respective processed simulated frames in horizontal axis in (b) and (d), and vertical axis in (f).

When the number of bins increases, the simulator will have a bigger scene frame to compute, and generate the sonar data.

5. Conclusion and future work

A GPU-based approach for imaging sonar simulation is presented here. The same model was able to reproduce the operation mode of two different types of sonar devices (FLS and

Table 2: Processing time to generate forward-looking sonar frames with different parameters.

# of samples	# of beams	# of bins	Field of view	Average time (ms)	Std dev (ms)	Frame rate (fps)
500	128	500	120° x 20°	54.7	3.7	18.3
500	128	1000	120° x 20°	72.3	8.9	13.8
500	256	500	120° x 20°	198.7	17.1	5.0
500	256	1000	120° x 20°	218.2	11.9	4.6
500	128	500	90° x 15°	77.4	11.8	12.9
500	128	1000	90° x 15°	94.6	10.2	10.6
500	256	500	90° x 15°	260.8	18.5	3.8
500	256	1000	90° x 15°	268.7	16.7	3.7

Table 3: Processing time to generate mechanical scanning imaging sonar samples with different parameters.

# of samples	# of bins	Field of view	Average time (ms)	Std dev (ms)	Frame rate (fps)
500	500	3° x 35°	8.8	0.7	113.4
500	1000	3° x 35°	34.5	1.6	29.0
500	500	2° x 20°	10.3	0.6	96.7
500	1000	2° x 20°	41.7	3.7	24.0

MSIS) over different scenarios. The real sonar image singularities, such as multiplicative noise, surface properties and acoustic shadows are addressed and represented in the simulated frames. Specially for the shadows, the acoustic representation can present information as useful as the insonified object. Considering the qualitative results, the sonar simulator can be used by feature detection algorithms, based on corners, lines and shapes. Also, the computation time to build one sonar frame was calculated using different device settings. The vertex and fragment processing during the underwater scene rendering accelerates the sonar image building, and the metrics, such as the average time, demonstrated that the performance is much close to real imaging devices. These results allowed the use of this imaging sonar simulator by real-time applications, such as obstacle detection and avoidance, and object tracking. Finally, the reverberation effect is still missing on our simulator to perform a more realistic sensing. The future inclusion of this phenomenon will probably change the reflected intensity model and the computation time must be considered again. Next steps will focus on expand the underwater acoustic characteristics, such as additive noise and reverberation, and qualitative and computation-efficiency evaluations with other imaging sonar simulators and real images.

References

[1] Bell JM. Application of optical ray tracing techniques to the simulation of sonar images. Optical Engineering 1997;36(6):1806–13.

[2] Coiras E, Groen J. Simulation and 3d reconstruction of side-looking sonar images. In: Silva S, editor. Advances in Sonar Technology; chap. 1. In-Tech; 2009, p. 1–15.

[3] Guériot D, Sintes C. Forward looking sonar data simulation through tube tracing. In: MTS/IEEE OCEANS Conference. 2010, p. 1–6.

[4] Saç H, Leblebicioğlu K, Bozdağı Akar G. 2d high-frequency forward-looking sonar simulator based on continuous surfaces approach. Turkish Journal of Electrical Engineering and Computer Sciences 2015;23(1):2289–303.

[5] DeMarco K, West M, Howard A. A computationally-efficient 2d imaging sonar model for underwater robotics simulations in Gazebo. In: MTS/IEEE OCEANS Conference. 2015, p. 1–8.

[6] Gu J, Joe H, Yu SC. Development of image sonar simulator for underwater object recognition. In: MTS/IEEE OCEANS Conference. 2013, p. 1–6.

[7] Kwak S, Ji Y, Yamashita A, Asama H. Development of acoustic camera-imaging simulator based on novel model. In: IEEE International Conference on Environment and Electrical Engineering (EEEIC). 2015, p. 1719–24.

[8] Quigley M, Conley K, Gerkey BP, Faust J, Foote T, Leibs J, et al. ROS: an open-source robot operating system. In: Workshop on Open Source Software, held at IEEE International Conference on Robotics and Automation (ICRA). 2009, p. 1–6.

[9] Hurtós N. Forwad-looking sonar mosaicing for underwater environments. Ph.D. thesis; Universitat de Girona; 2014.

[10] Abbot J, Thurstone F. Acoustic speckle: theory and experimental analysis. Ultrasonic Imaging 1979;1(4):303–24.

[11] Ganesan V, Chitre M, Brekke E. Robust underwater obstacle detection and collision avoidance. Autonomous Robots 2015;40(7):1–21.

[12] Ribas D, Ridao P, Neira J. Underwater SLAM for structured environments using an imaging sonar. Springer-Verlag Berlin Heidelberg; 2010.

[13] Fallon MF, Folkesson J, McClelland H, Leonard JJ. Relocating underwater features autonomously using sonar-based SLAM. Journal of Ocean Engineering 2013;38(3):500–13.

[14] Liu L, Xu W, Bian H. A LBF-associated contour tracking method for underwater targets tracking. In: MTS/IEEE OCEANS Conference. 2016, p. 1–5.

[15] Huang TA, Kaess M. Towards acoustic structure from motion for imaging sonar. In: IEEE/RSJ International Conference on Intelligent Robots and Systems (IROS). 2015, p. 758–65.

[16] Bradski G. The opencv library. Doctor Dobbs Journal 2000;25(11):120–6.

[17] Watanabe T, Neves G, Cerqueira R, Trocoli T, Reis M, Joyeux S, et al. The Rock-Gazebo integration and a real-time AUV simulation. In: IEEE Latin American Robotics Symposium (LARS). 2015, p. 132–8.

[18] SDF. `http://sdformat.org/`; 2017. Accessed: 2017-04-23.

[19] Soetens P, Bruyninckx H. Realtime hybrid task-based control for robots and machine tools. In: IEEE International Conference on Robotics and

Automation (ICRA). 2005, p. 260–5.
[20] Rost RJ, Licea-Kane B, Ginsburg D, Kessenich JM, Lichtenbelt B, Malan H, et al. OpenGL shading language. 3rd ed.; Addison-Wesley Professional; 2009.
[21] Lee J. Digital image enhancement and noise filtering by use of local statistics. IEEE Transactions on Pattern Analysis and Machine Intelligence 1980;2(2):165–8.